Joint Centre for Mesoscale Meteorology, Reading, UK

Release of potential shearing instability in warm frontal zones

K. A. Browning
D. Chapman

Internal Report No. 83

February 1998

Met Office Joint Centre for Mesoscale Meteorology Department of Meteorology
University of Reading PO Box 243 Reading RG6 6BB United Kingdom
Tel: +44 (0)118 931 8425 Fax: +44 (0)118 931 8791
www.metoffice.com

Designed and produced by the Met Office © Crown copyright 2001 01/0240 The Met Office logo is a registered trademark.

Release of potential shearing instability in warm frontal zones

D. Chapman and K. A. Browning*

February 12, 1998

Summary

Potential shearing instability (PSHI) exists in the atmosphere when the Richardson Number in a stably stratified shear layer would be less than $\frac{1}{4}$ if the layer were lifted to saturation. Sometimes the air entering a warm frontal zone near the position of the surface warm front is initially unsaturated, its Richardson Number is greater than $\frac{1}{4}$, but PSHI exists over a deep layer. This paper presents a study of a warm frontal zone using observations from the high-resolution Doppler radar at Chilbolton supported by radiosondes and output from the Mesoscale version of the operational U. K. Met. Office Unified Model. Very large-amplitude Kelvin-Helmholtz billows were observed to form where the PSHI was realised following the onset of saturation. The billows were probably intense enough to be a hazard for air traffic and an important source of momentum transfer. Rough estimates from the radar of vertical momentum fluxes due to the billows are shown to be broadly consistent with measurements by the same radar of the change in velocity profile across the frontal zone from start to end of the billow train. The present version of the Unified Model does not parameterize vertical mixing due to shearing instability in the free atmosphere; this may be an important omission.

*Corresponding author: Joint Centre for Mesoscale Meteorology, Department of Meteorology, University of Reading, Whiteknights Road, PO Box 243, Reading, Berkshire, RG6 6BB, UK. (The Joint Centre for Mesoscale Meteorology is supported by the Meteorological Office and the Department of Meteorology, University of Reading.)

1 Introduction

Over the last 30 years, the existence of billows in the atmosphere has been demonstrated from aircraft (Browning *et al.* 1973a; Hardy *et al.* 1973; Nielsen 1992) and radar (Atlas *et al.* 1970; Browning 1971; James and Browning 1981) measurements, and by visual observation of associated clouds (e.g. Ludlam 1967, 1980). The existence of large-amplitude billows in the atmosphere has been established primarily by observations using radar (e.g. Browning 1971). Such billows, with wavelengths up to 5 km and vertical depths of the order of 1 km, have been considered mainly as a concern to aviation safety by causing clear air turbulence (CAT). However, billows also mix across their depth and dissipate kinetic energy (Bryant and Browning 1975; Kennedy and Shapiro 1979), so they could have a significant effect on the larger scale features in which they are embedded, such as a jet stream or frontal zone.

Billows observed in the atmosphere (for examples, see Gossard 1990) occur across layers of stratified shear and tend to have a structure very similar to that found in laboratory tank experiments (Thorpe 1975, 1987) and numerical models (Sykes and Lewellen 1982; Scinocca 1995; Fritts *et al.* 1996) of the Kelvin-Helmholtz instability (e.g. Drazin and Reid 1981; Readings 1973). This instability occurs when a stably stratified transition layer between two fluids of different density is rolled up by a shear across the layer, forming billows orientated at right angles to the shear. The stability of the layer is governed by the Richardson number, Ri, defined by N^2/S^2 where N is the Brunt-Väisälä frequency, and S is the vertical wind shear. A necessary, but not sufficient condition for instability is that $Ri < \frac{1}{4}$ somewhere in the flow (Miles and Howard 1964). Although the exact criterion depends on the profiles of N and S, in practice the atmosphere will be unstable if Ri falls much below $\frac{1}{4}$. Observations using high-power radar which detects regions of high refractive index variance to delineate billows occuring in clear air, show that billows occur where $Ri \approx \frac{1}{4}$ (e.g. Browning 1971). The value of Ri depends critically on the depth of the layer over which it is measured and so it is significant that the measurements by Browning were for large-amplitude billows which occurred over depths large enough to be resolved by the radiosondes used.

This paper builds on an initial study by Chapman and Browning (1997) (hereafter referred to as CB), and addresses two questions regarding large-amplitude billows in the atmosphere. Firstly, what causes large-amplitude billows to occur where they do? Roach (1970), Bosart and Garcia (1974) and Keller (1989) have attempted, with mixed success, to relate areas containing billows and CAT to indices diagnosed from larger-scale properties of the flow in the upper troposphere. Billows may also occur due to vertically propagating gravity waves breaking at their critical level (e.g. Fritts and Garten 1996), possibly in a location related to the orography. Here we suggest that, in addition to these locations, billows may be a fairly common (but largely unobserved) feature of surface warm fronts.

The second question is what is the meteorological significance, i.e., up-scale effect, of the billows. Although the relevance to aviation safety has been established, their direct effect on atmospheric profiles through vertical fluxes of temperature and momentum has been measured to any significant extent only within or at the top of the boundary layer (e.g. Metcalf and Atlas 1973; Blumen 1984), where billows generally have a smaller wavelength and depth. In this study, high-resolution Doppler radar data through billows has allowed the three-dimensional flow field to be calculated, which has in turn yielded vertical fluxes of momentum. Although the flux estimates are subject to considerable error they nevertheless

imply a change in the vertical profile of wind velocity that is consistent with the change directly observed upstream and downstream of the billows.

We shall show that the role of moisture at the front is important, both in causing billows to occur, and in enabling them to have a large depth (comparable with the depth of the frontal zone itself). Thus large-amplitude billows may cause considerable vertical mixing within a significant proportion warm fronts, and this mixing may itself substantially alter the structure of the frontal zone. This case study demonstrates the existence of a latent shearing instability, which is released when a layer is lifted to saturation. We refer to this as potential shearing instability (PSHI).

2 The Nature of the Billows and the Radar Data

(a) The Chilbolton Radar

Observations were made using the 3 GHz multi-parameter radar (Goddard *et al.* 1994) at Chilbolton (51.15°N, 1.44°W) which is approximately 80 km north of the south coast of England. The radar has a peak power of 560 kW. The observations were made within light precipitation and this enabled the billows to be detected at longer ranges than is possible in the clear air. The data have a range resolution of 300 m which is achieved by range-averaging over groups of four gates, each 75 m in length. The dish is 25 m in diameter, giving an angular resolution of 0.28°. This is an unusually high angular resolution for a 10 cm wavelength radar. It allows the presence of billows similar to those described below to be identified (given precipitation to render them detectable) out to a range of around 80 km, although the data beyond a range of around 50 km do not resolve much quantitative information on the structure of billows.

(b) General properties of the radar data collected within billows

Data were collected continuously during the passage of a strong warm frontal zone, between 1600 and 2300 UTC on 6 September 1995. The data were in the form of both RHIs (**R**ange **H**eight **I**ndicators) and PPIs (**P**lan **P**osition **I**ndicators). In RHIs the radar beam is scanned at different elevations in a fixed bearing (azimuth) - equivalent to a cross-section through the atmosphere in a vertical plane passing through the radar. In PPIs the radar beam is scanned in azimuth at a fixed (normally low) elevation. Decisions concerning where to scan were made as the data were acquired, depending on the nature of the data at the time, rather than following a predetermined pattern of RHIs and PPIs.

When the radar is scanned at low elevations the Doppler velocity of precipitation targets yields the line-of-sight horizontal wind component, essentially uncontaminated by the vertical fall-speed of the precipitation (the majority of the data used were from elevations below 5°; at this elevation the error is around 0.5 m s^{-1}). Thus the air motion within the frontal zone and associated billows can be seen clearly in the Doppler data. The billows also appeared to induce small drizzle shower clouds in a convectively unstable region which existed just above the frontal layer containing the billows (refer ahead to Fig. 8(a) for evidence of potential instability). These showers then produced weak reflectivity cores orientated

parallel to the billows, but travelling at the air velocity above the shear layer, so moving out of phase with the billows. For the purposes of this study, all further discussion of the Chilbolton radar data will refer only to the strongly sheared warm frontal zone rather than the overlying convection, and to the Doppler data as opposed to the reflectivity data.

Billows were observed in the radar data between 2005 and 2050 UTC when scans were made at intervals of 5° between azimuths 210 and 270°, and again between 2200 and 2240 UTC when scans were made between azimuths 0 and 90°. Between these two periods scans were made in all general directions but only at ranges greater than 50 km, and no billows were observed, although billows are presumed to have continued to exist during this interval but to have been unobserved because of the ranges scanned.

The billows were orientated with their axes almost due south-north. Examples of RHIs orientated at right angles to their axes (i.e., at an azimuth of 90°) are shown in Fig. 1(a)-(c). In addition to the field of Doppler velocity (a), two derived fields are shown. These are (b) the vertical wind shear, clearly showing the structure and extent of the billows, and (c) a streamfunction which indicates air parcel streamlines projected onto the plane of the diagram (for more details of the derivation of the streamfunction, see CB). Labels on the closed streamfunction contours indicate the time taken in minutes for air parcels to complete a circuit. Figures 1(d) and (e) show an example of similar billows observed in another warm frontal zone on 11 February 1997. This case will be discussed further in section 5, but most of the paper will deal with the September case previously studied by CB.

A schematic diagram showing the location and orientation of billows relative to the front with which they were associated is shown in Fig. 2 (quantitative aspects are discussed later). The locations of billow "crests" were determined subjectively from peaks of Doppler velocity in RHIs such as Fig. 1(a). The surface front itself, as defined by sharp gradients in the wind field from radar observations, moved northwards at around 10 m s^{-1}. As this figure shows, the radar was capable of resolving the billows well only at close range, as they passed close to the radar site. It seems likely that billows existed along other parts of the front (in a strip moving with the surface front, continuing beyond the range of the radar) and also at earlier times, when this strip was beyond the range of the radar. Owing to the nature of the air flow within the billows, they are most evident in the Doppler data when observations are made perpendicular to their axes. There is no Doppler evidence of them when observations are made along their length.

A hodograph derived from two Doppler velocity RHIs separated by 45° within the billows (averaged over two billow wavelengths) was shown in Fig. 3 of CB. The main features of the hodograph are represented by the two vectors shown in Fig. 2 of the present paper. The billows were orientated perpendicular to the main shear between 0.4 and 1.6 km. There was a mean southerly wind of around 20 m s^{-1} at the height of the billows and since the billow train was travelling northwards with the warm frontal zone at 10 m s^{-1}, the component of flow within the billows along their axes was at a relative speed of 10 m s^{-1}. Thus the closed streamlines in Fig. 1(c) represent approximately helical air-parcel trajectories in the core of the billows. The time taken for an air parcel to complete a circuit (i.e., for the air to completely overturn) within the billows was approximately 20 minutes, assuming that the streamlines shown are representative of the billows along all their length.

East-west scans were made by the radar as the train of billows advanced northwards, towards and then over the radar site. Just before the billows reached the radar, the observations

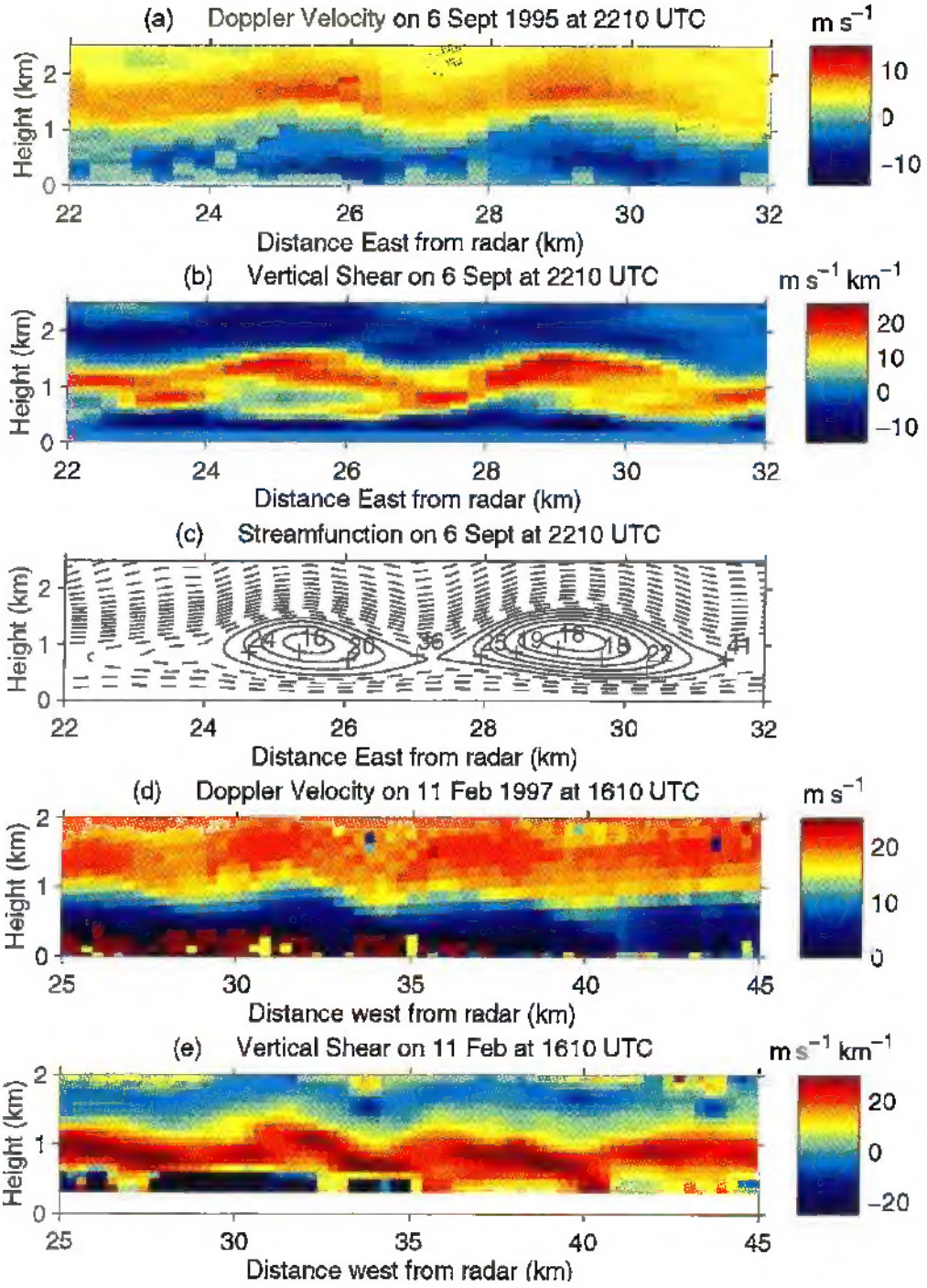

Figure 1: (a)-(c): RHIs obtained at 2210 UTC on 6 Sept. 1995 at an azimuth of 90° through billows showing (a) Doppler velocity, u (m s^{-1}), positive values indicating air flow to the east, (b) vertical shear, du/dz (m s^{-1} km^{-1}) and (c) mass-weighted streamfunction (intervals of 500 kg m^{-1} s^{-1}) indicating parcel streamlines in this plane; details are discussed in the text. (d) and (e) show the Doppler velocity and vertical shear through billows observed at 1610 UTC on 11 Feb. 1997. The patterns in these two RHIs are not as clear as in the first three because scans could not be made exactly perpendicular to the billow axes.

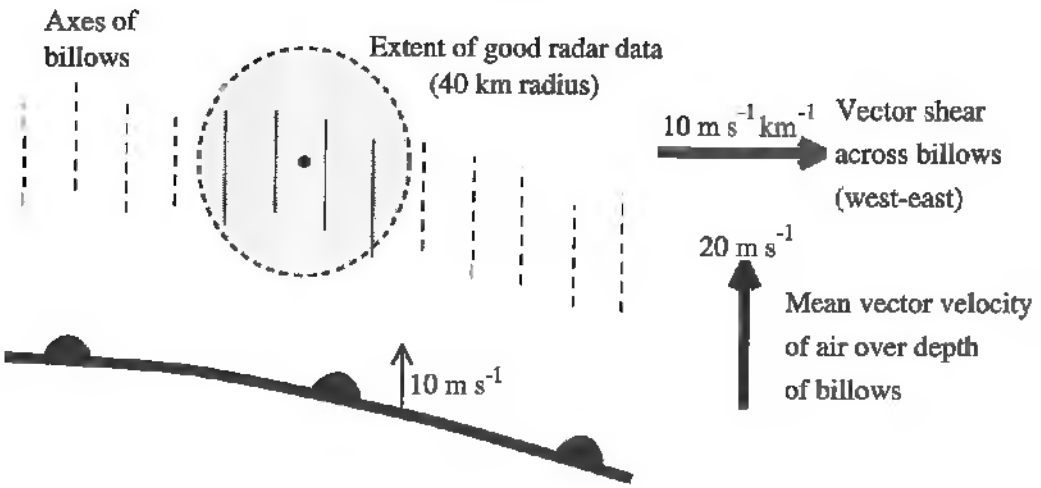

Figure 2: Schematic diagram showing the extent of radar coverage, the observed location of billow axes (shown by solid lines) and the likely location of the billows (dashed lines) in relation to the surface warm front.

were therefore just downwind (north) of the billows. Later (e.g. Fig. 1(a)), while the train of billows was above the radar, observations were made within the billows themselves. The vertical extent of the layer containing a positive west-east component of shear (averaged over an integral number of wavelengths) was 0.4 to 1.7 km within, and 0.5 to 2.5 km just downwind of the billows. Their wavelength was between 4 and 5 km. There was considerable variation in the along-axis length of the billows, ranging from around 10 to 40 km. An accurate measurement of the mean length could not be made, as many of the billows lay partly outside the region scanned by the radar, but a subjective estimation of around 30 km is reasonable. The train of billows as a whole had a south-north extent slightly greater, around 40 km, due to variation in the location of individual billows. The overall train of billows existed for all the time that the radar was capable of observing them (3 hours). This is considerably longer than the residence time of air parcels within individual billows which, since the air was moving along their axes at a relative speed of 10 m s^{-1}, was around 50 minutes. Browning and Watkins (1970) observed billows of a similar amplitude complete their lifecycle over a period of 10 minutes. Evidently the larger-scale flow was acting to sustain the shearing instability over a longer period in the present study.

3 Use of mesoscale model to determine role of mesoscale structure in determining location of billows

(a) The mesoscale model

The U. K. Meteorological Office Unified Model is described by Cullen (1993). To summarise, the mesoscale model uses a hybrid vertical coordinate which is terrain-following in the lower layers of the atmosphere. It has 31 levels in the vertical, with a resolution of around 40 m at the surface, and 300 m at an altitude of 2 km. A regular latitude-longitude grid is used in the horizontal, with a resolution of around 17 km. It takes its lateral boundary conditions

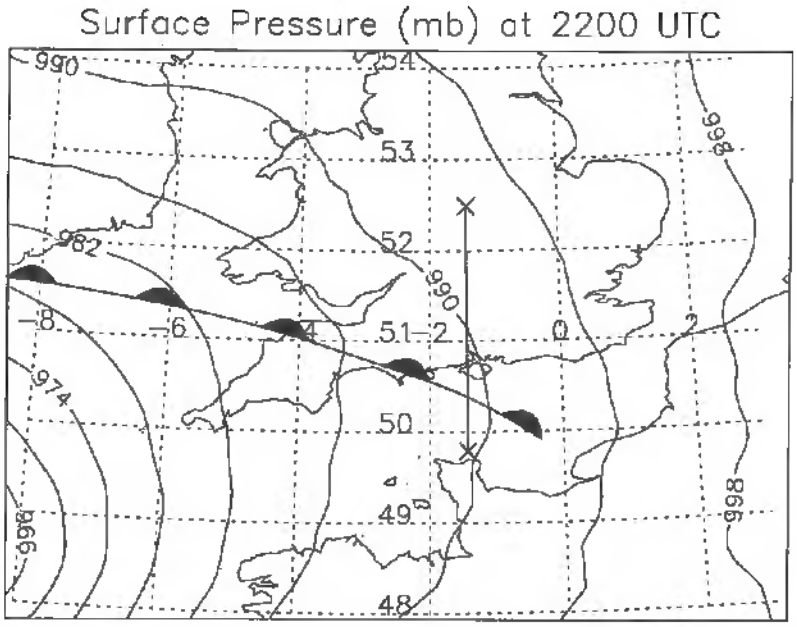

Figure 3: Mean sea-level pressure and the analysed position of the surface warm front from a 4-hour forecast by the mesoscale model, valid at 2200 UTC, 6 Sept. 1995. XX shows the position of the cross-sections in Fig. 4.

from a coarser-resolution limited-area model in which it is nested. In the boundary layer, vertical turbulent transport of quantities is calculated depending on the local Richardson number. These transports are calculated taking into account the presence or absence of cloud. Outside of the boundary layer there is no such calculation, and no artificial vertical diffusion.

The data used in this study are from the 1800 UTC operational run of the model on 6 Sept. 1995. As comparisons between the model and observations are made at 2200 UTC, this allows the model 4 hours to "spin up" to give a realistic representation of the atmosphere.

(b) The warm frontal structure as determined by the mesoscale model

A plan view showing the mean sea-level pressure and the analysed surface warm front (SWF) at 2200 UTC is given in Fig. 3. This figure also shows the location of south-north cross-sections of model data centered on Chilbolton radar which are given in Fig. 4(a)-(d). These show details of wet bulb potential temperature (θ_w), relative humidity (RH), west-east component of the wind (u), and front-relative wind arrows projected onto this section. They indicate the following features of the front:

- Warm, moist air approached the SWF at low levels (below 1 km) from the south, and then rode up over the frontal zone, retaining an eastward component as it did so.
- Cold, and initially dry air ahead of the surface warm frontal zone travelled westwards, approaching it at low levels. As it entered the lower part of the frontal zone, it rose and then moved northwards retaining its westward component as it did so.

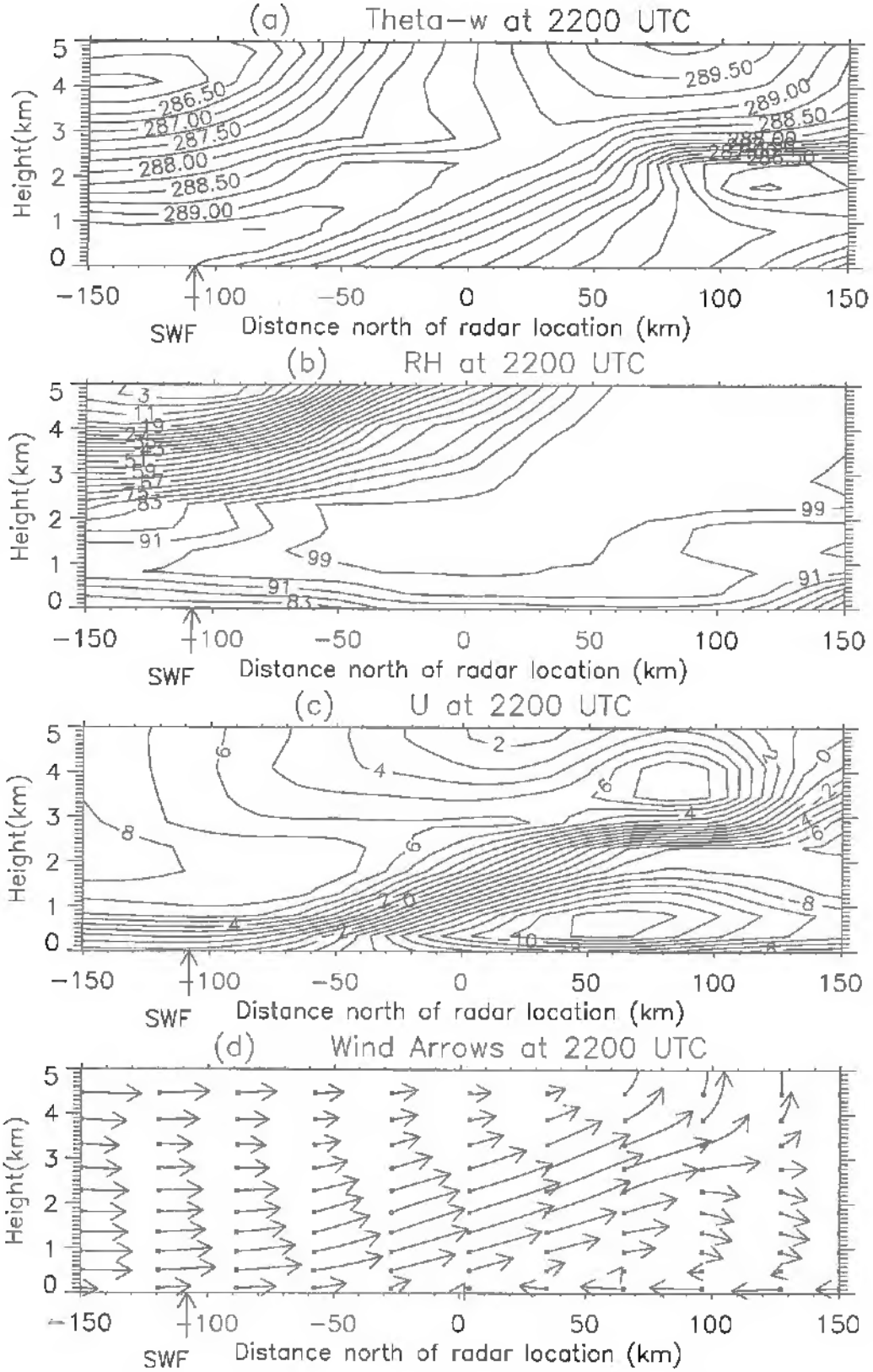

Figure 4: Vertical cross-sections from the mesoscale model at 2200 UTC, 6 Sept. 1995 along the line XX in Fig. 3 which passes through Chilbolton radar. (a): Wet-bulb potential temperature, θ_w (K). (b): Relative humidity with resepct to ice (%). (c): West-east component of the wind, u (m s^{-1}, +ve out of the plane). (d): Front-relative wind arrows, the length of each indicating parcel displacements over a period of 1 hour.

- Air within the frontal zone itself originated mainly from the boundary layer just ahead of the SWF.
- The warm and cold air had a relative motion that was broadly consistent with the thermal wind relation, so the change from an easterly to westerly component with height just north of the SWF was related to the temperature gradient across the front.

An upper cold front (UCF) existed ahead of the SWF, with banding in the cloud and precipitation similar to that described by Browning *et al.* (1973b). Behind the UCF the dry low-θ_w air overriding the moist warm-sector air gave rise to potential instability. The convective cells referred to earlier were due to the release of this potential instability, but this is incidental to the main theme of the paper.

(c) Validation of the larger-scale thermodynamic features reproduced by the model

Figure 5 shows time–height plots of θ_w, from (a) the mesoscale model and (b) radiosonde data from Herstmonceaux, both at 0.3°E, 50.9°N, 120 km to the east of the sections in Fig. 5. Warm air is shown shaded in the section from the model. The two sections show good agreement in the following respects:

- The SWF passes over Herstmonceaux at the same time (0200 UTC $\pm$ 1 h).
- θ_w at the SWF is within 0.5 K of 288.5 K.
- The ascent at 2000 UTC gives a similar depth between 287 and 289 K through the front, although the layer between these two temperatures in the model is slightly higher and deeper.

Thus the model is interpreted as having reproduced actual thermodynamic structures well, locating them to within around $\pm$ 90 minutes. This corresponds to a distance of approximately 55 km, which is 3 model grid lengths.

(d) The model's detailed representation of the frontal zone and the adjustments required to fit the observations

Section 3(c) has demonstrated that the model and the observations were broadly consistent. However, in order to relate the radar observations of the billows to the model we need to obtain consistency on scales of order 10 km. The aim of this section is to show how the model, which yields both thermodynamic and kinematic fields, has been adjusted slightly so that it is consistent on these scales with the kinematic fields obtained from the radar, and other observations. This adjustment has been done to obtain the "best estimate" of the state of the atmosphere at the exact time and place where the billows are known to have existed.

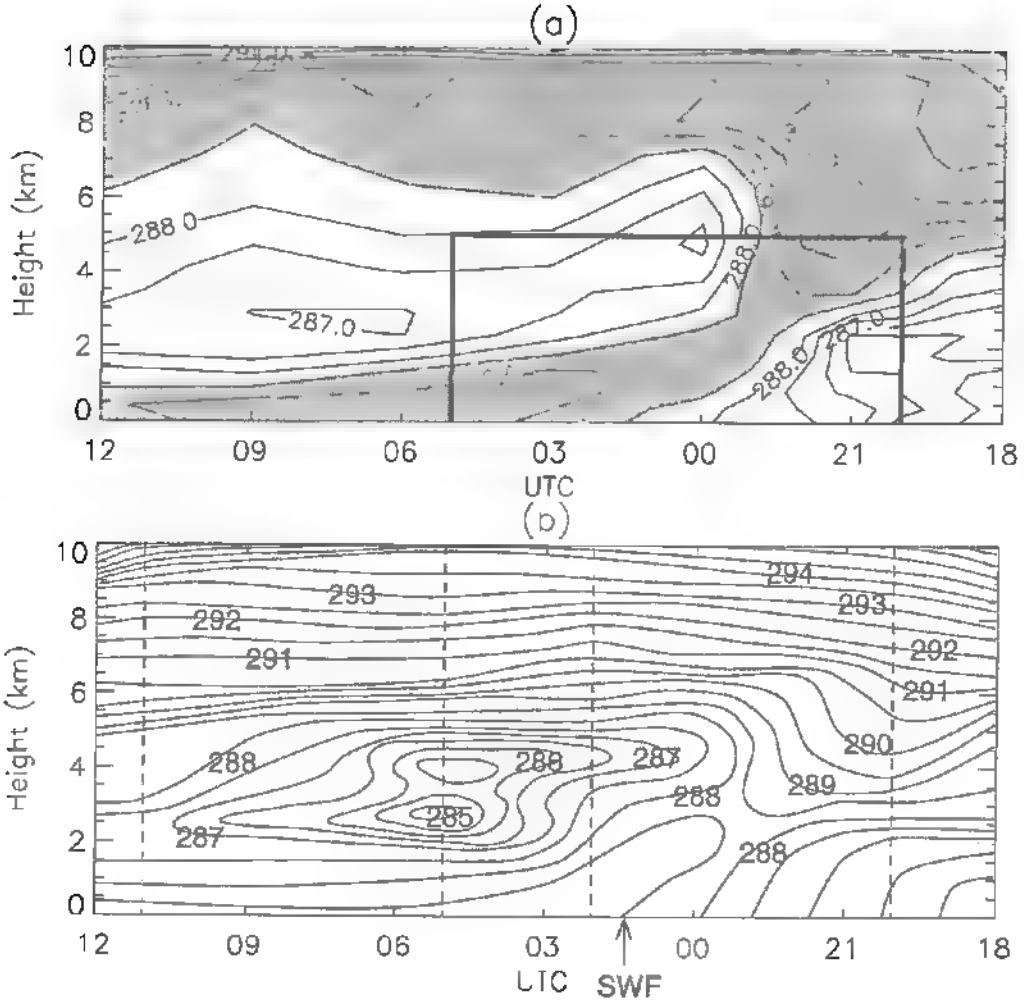

Figure 5: Time-height sections of θ_w above Herstmonceaux on 6/7 Sept. 1995, derived from (a) mesoscale model and (b) radiosonde ascents. The warm air (θ_w > 288.5K) is shown shaded in (a). The times of radiosonde ascents are indicated by the dashed lines in (b). Owing to the sparcity of data in some regions of (b) the mesoscale model has been used to help interpolate the radiosonde data in a realistic way (although the contours still fit the radiosonde data at the times of ascents). The equivalent location of distance-height cross-sections in Figs. 4, 6 and 8 are shown by the rectangle in (a).

(i) *Comparison of the model's southerly wind component (v) with that measured by the radar.* Figure 6 shows a cross-section of the southerly (front-normal) component of wind from the model and radar at 2200 UTC. The main feature is the low-level "jet" of warm air which rides up over the frontal zone. In the model and radar data, this jet has a similar shape, slope and magnitude, with a maximum of around 20 m s^{-1}. However, the location of the jet axis is displaced in the model relative to the radar. This displacement could be due to the model having located the frontal system (i) too far south by approximately 40 km, or (ii) too high by approximately 800 m, or a combination of (i) and (ii). Evidence given below in Section 3(d)(ii) suggests that (i) is more likely.

(ii) *Comparison of the model's westerly component of the wind shear ($\partial u/\partial z$) with that measured by the radar.* We compare in Fig. 7 the wind shear profile ($\partial u/\partial z$) derived from radar data within the billows with the two corresponding model wind shear profiles derived assuming (i) and (ii) above respectively. The radar observations (Fig. 7(c)) show a maximum in the vertical wind shear at a height of 1.2 km. The corresponding maximum occurs at

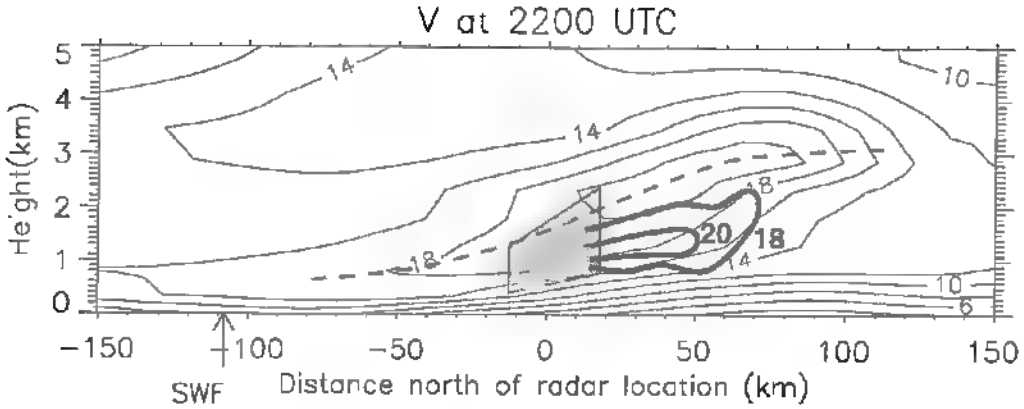

Figure 6: South-north cross-section at 2200 UTC, 6 Sept. 1995, along the line XX in Fig. 3 showing the southerly component of wind, v (m s^{-1}) from the mesoscale model (thin lines). The model's jet axis is shown dashed. Superimposed are two contours (18 and 20 m s^{-1}) of the same component of the wind measured by the radar (bold lines). The location of the billows is shown shaded.

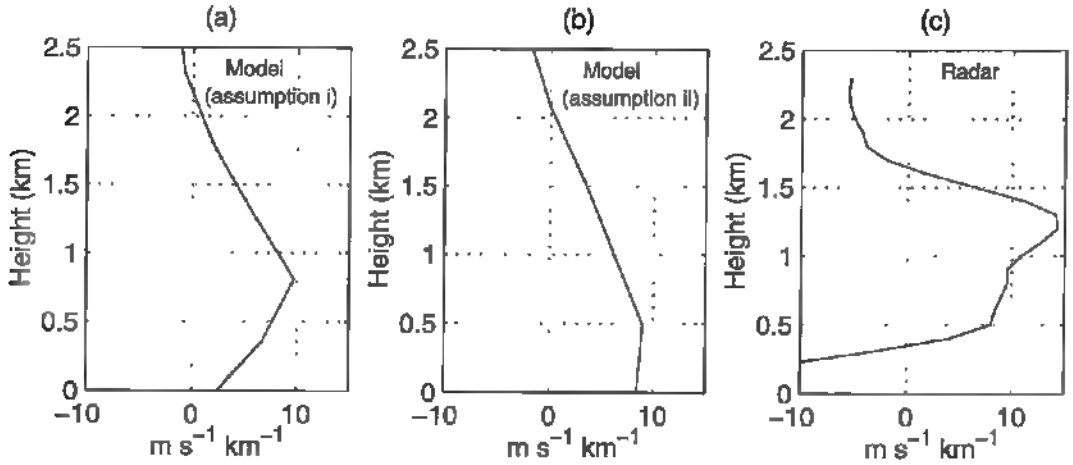

Figure 7: Vertical profiles of the westerly component of the vertical wind shear ($\partial u/\partial z$) at 2200 UTC, 6 Sept. 1995, in the region of the billows. (a) and (b): Model-derived profiles obtained after adjusting the model according to assumptions (i) and (ii), respectively (see text). (c): Radar-derived profile based on radar data averaged over times 2200, 2210 and 2220 UTC, and averaged over 12 km close to the radar.

heights of 0.8 km and 0.5 km in Figs. 7(a) and (b) respectively. The closer fit of (a) supports assumption (i), implying that the model mislocated the front by around 40 km to the south. This is consistent with the resolution of the model, as a displacement of 40 km horizontally implies an error of only 2 grid lengths. However, there are 4 model levels between 1.0 and 1.8 km, so a vertical displacement seems less appropriate in any case.

In addition, the shear layer responsible for the billows was spread out over a greater depth in the model. As a consequence, the peak shear was only around 10 m s^{-1} km^{-1} in the model (Fig. 7(a)) compared to 14 m s^{-1} km^{-1} in the profile derived from the radar data (Fig. 7(c)).

(iii) *Comparison of the model's relative humidity with observations from synoptic reporting stations.* As we shall see later, the behaviour of the billows depended critically on the level of saturation (i.e., the cloud base) and so it is important to adjust any small errors that there may have been in the model's relative humidity field, especially at low levels where the billows occurred. The model cross-section showing RH in Fig. 4(c) indicates a cloud

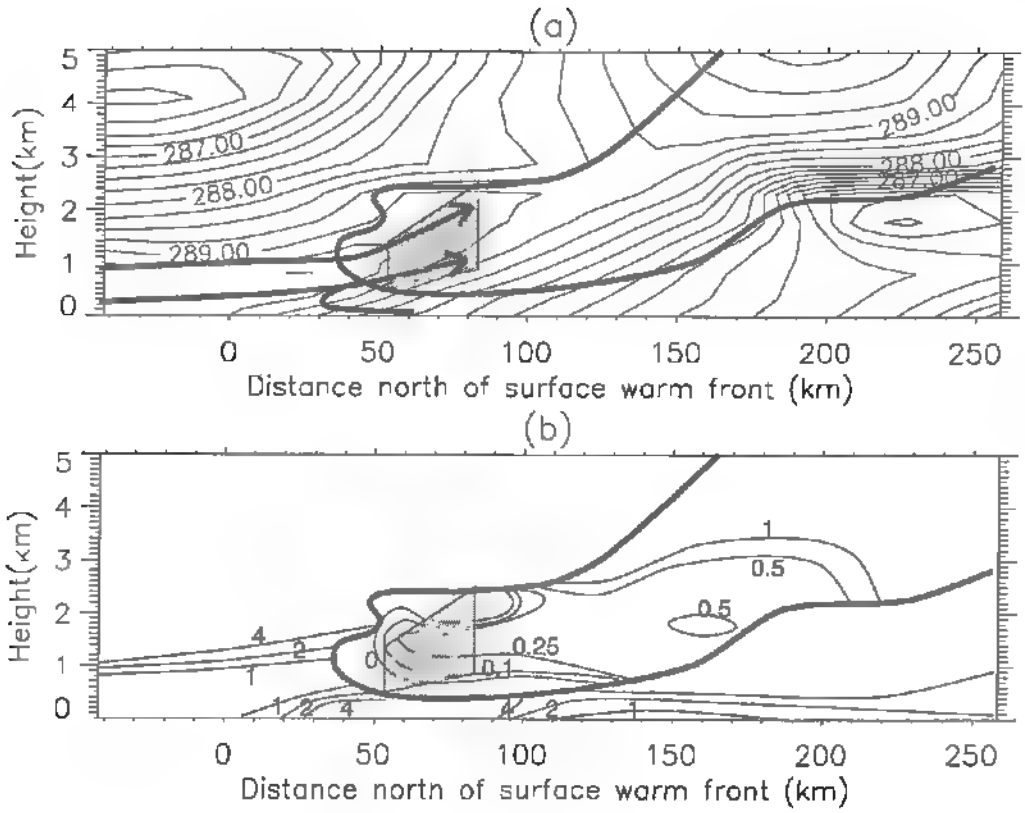

Figure 8: South-north vertical cross-sections (passing through Chilbolton radar) at 2200 UTC, 6 Sept. 1995, showing fields adjusted as described in the text. The fields shown are (a) wet-bulb potential temperature and front relative streamlines entering the region containing the billows and (b) Richardson number Ri_x as defined in the text. The effective region of saturation (RH>99%) is delineated by a bold contour, and the location of the billows is shows shaded, in both (a) and (b).

base, assuming that this is given by the 99% contour, at around 900m. However, synoptic observations at this time indicate that the cloud base north of the SWF was lower than this, at approximately 400m.

(iv) *Adjustment of the model fields.* Section 3(c) has validated the model on scales greater than 100 km horizontally, and 500 m vertically. The comparisons made in Sections 3(d)(ii) and 3(d)(iii) indicate the need for all of the following finer scale adjustments:

- displace all model fields 40 km north to agree with Doppler radar observations of the kinematic structure of the front
- increase model shear by a factor of 1.4 in the frontal zone, to agree with radar observations of the shear responsible for the billows
- reduce height of $RH = 99\%$ contour by 400 m to around 400 m, to agree with cloud base observations.

By adjusting the model output in this way, the resulting fields will be more accurate (though less balanced) than the raw model fields, and of course much more comprehensive than the actual observations. The discrepancy that is introduced in the location of the northern end

of the south-north jet may be explained as the result of the mixing induced by the billows not being represented by the model.

Figure 8(a) shows the resulting adjusted model fields of θ_w and $RH = 99\%$ in the region of the surface warm front, including the location of the observed billows and the front-relative airflow into them. The causal relationship between these fields and the location of the billows will be discussed in Section 3(b).

(e) Calculation of the Richardson number

The Richardson number is defined as the ratio of the static stability to the vertical wind shear. However, in this case the evaluation of Ri appropriate to the billow formation is complicated by two factors: (i) the proximity of the frontal shear zone to the strong differently orientated shear in the boundary layer, and (ii) the saturation of much of the frontal zone.

(i) *The problem of the variable orientation of the shear vector.* The hodograph shown in Fig. 3 of CB indicates that there was a strong south-north component of wind shear between the ground and a height of 0.6 km, which would have been associated with relatively small-scale turbulent mixing in the boundary layer. The strong west-east component of shear responsible for the observed large-amplitude billows existed between 0.4 and 1.6 km. Although the lower portion of the billow shear layer, between 0.4 and 0.6 km, slightly overlapped with the boundary layer induced shear, most of the billow layer, between 0.6 and 1.6 km, was characterized by an almost zero component of shear in the south-north direction. The south-north component of the wind shear has been neglected in the following calculations of Ri since it is only the instability of the flow to large-amplitude billows that we are concerned with in this study. By calculating Ri_x rather than Ri we greatly increase the apparent Richardson Number in the boundary layer, but the value in the frontal zone is close to the actual Richardson Number because of the very small south north component of shear over the layer containing billows.

(ii) *The effect of saturation on the static stability.* The static stability has been defined as

$$N^2 = N_d^2 = \frac{g}{\overline{T}}\left(\frac{dT}{dz} - \Gamma_d\right) - \frac{g}{\overline{\theta}}\frac{d\theta}{dz} \tag{1}$$

where the air is unsaturated (RH <99%). However, for a given temperature profile, the atmosphere will always have a reduced static stability if it is made saturated, due respectively to the release and absorption of latent heat accompanying upward and downward air-parcel displacements. Although for large vertical displacements the evaporation of water droplets may be too slow to maintain saturation, it is reasonable to assume that, in the early stages of the growth of an instability, small downward displacements by an air parcel can maintain saturation by rapid evaporation of the smallest cloud droplets. In regions where the air is saturated (RH >99%) the static stability has been defined as (Lalas and Einaudi 1974)

$$N^2 = N_w^2 = \frac{g}{\overline{T}}\left(\frac{dT}{dz} - \Gamma_w\right)\left(1 + \frac{Lq_s}{RT}\right) - \frac{g}{1+q_w}\frac{dq_w}{dz} \tag{2}$$

This expression for N_w^2 was shown by Durran and Klemp (1982) to be a good approximation to the correct value, and a much better approximation than that obtained by a simple substitution of θ_w for θ in (1).

Ri_x was calculated at 50 mb intervals, over depths of 100 mb (corresponding to a height interval of around 800 m), which is comparable to the observed depth of the billows. The result is shown in Fig. 8(b). The different definitions of N^2 in the saturated and unsaturated regions lead to the discontinuities at the cloud boundary.

(f) The aspects of the mesoscale frontal structure that determined the location of billows

Figure 8 shows the best estimate of the relevant thermodynamic and kinematic fields in the frontal zone at the time of the billows. The processes leading to the development of the billows can be inferred from these fields.

High-θ_w air which approached the frontal zone from behind (ie south of) the surface front (upper bold arrow in Fig. 8(a)) was initially unsaturated. Ascent occurred in association with convergence near the surface front, and above 500 m the air became saturated as it flowed northwards. Lower θ_w air which approached the frontal zone at low levels (in the boundary layer) from the north was also unsaturated. Close to the surface front, this air mixed with warmer air and then it too ascended (lower bold arrow in Fig. 8(a)), becoming saturated as it travelled upward and northward conserving its θ_w.

These two air-streams, represented by the two bold arrows in Fig. 8(a), were in relative motion in the direction perpendicular to the cross-section, broadly in agreement with the thermal wind relation. This gave rise to the strong shear layer between them. This is the shear layer that caused the large-amplitude billows to occur. If the air had been dry, then the sheared layer would have had a minimum Richardson number of around 1 over a depth of 800 m. However, the air was saturated, and so the layer had a Richardson number of between 0 and $\frac{1}{4}$ when measured over 800 m increments (Fig. 8(b)), consistent with the observed occurrence of large-amplitude billows.

The location of initiation of billows in the frontal region, according to the analysis, was dictated by the height of the $RH = 99\%$ contour (although the height of this contour itself may in turn have been affected to some extent by the presence of the billows). Upstream of the billows, while the flow was still unsaturated, the shear was allowed to become large whilst the dry Richardson number remained well above $\frac{1}{4}$. The Richardson number when calculated assuming the air was moist in this location was, however, less than $\frac{1}{4}$. This potential for instability was then released "immediately" the air became saturated, initiating billows over a considerable vertical depth of 1 km, with an initial minimum Richardson number well below $\frac{1}{4}$.

4 The effect of the billows on the mesoscale frontal structure

(a) Introduction

The Doppler radar wind profiles within and downwind of the billows showed a considerable change over a south-north distance of around 30 km (see Figs. 5(a) and 5(b) in CB). Part of this change was due to the lifting of the overall frontal shear layer with distance ahead of the surface front. The other part of the change was due to the shear over the layer containing billows being redistributed over a greater depth. Although the nature of the change is consistent with it having been caused by the billows, it could alternatively be a feature of the larger-scale flow field. In Section 4(b), estimates are presented of the vertical profiles of the vertical flux of horizontal momentum due to the resolvable flow patterns associated with the large-amplitude billows. Although the estimates are prone to considerable error and do not constitute an adequate statistical sample, they tend to support the view that the billows themselves could have been responsible for the observed change in the wind profile over their length.

(b) Calculation of momentum flux from radar measurements

The Reynolds decomposition for data from point measurements is performed by separating fields into their time-mean and time-dependent parts, such that the time scales of the two parts are widely separated. However, in the present case, the data are in the form of spatial fields of the front-parallel (i.e., west-east) component of the wind and so the measurements are separated instead into their horizontal-mean and horizontal-dependent parts:

$$u = < u > + u^* \qquad\qquad w = < w > + w^*$$

where the mean is taken over an integral number of billow wavelengths.

When this decomposition is incorporated into the equations of motion, the term representing the effect of the billows on the mean flow is given by the Reynolds stress component in the front-parallel (x) direction, $-\rho < u^* w^* >$, which is the component of the momentum flux due to the billows. The effect of the billows on the mean flow is given by the momentum flux convergence, so

$$\frac{D < u >}{Dt} = -\frac{\partial < u^* w^* >}{\partial z} \tag{3}$$

where

$$\frac{D < u >}{Dt} = \frac{\partial < u >}{\partial t} + < v > \frac{\partial < u >}{\partial y}$$

Observations of the billows over three hours indicated that their location remained essentially fixed relative to the surface front, and their structure did not noticeably change. This implies that in a reference frame moving northwards with the front, then $\partial < u > / \partial t = 0$. Thus the term involving momentum fluxes can be directly related to observed changes in wind profiles from north to south:

$$\frac{\partial < u >}{\partial y} = -\frac{1}{v_{rel}} \frac{\partial < u^* w^* >}{\partial z} \tag{4}$$

where v_{rel} is the southerly component of the wind at the height of the billows relative to the front, equal to 10 m s^{-1}.

At 2210 UTC four billows which existed to the east of the radar were sampled. A plan view of these billows can be seen in Fig. 2 of CB. They were chosen because of their proximity to the radar, and lack of ground clutter in the radar data. These billows will be referred to as I, II ,III and IV, from west to east. The Doppler velocity in this direction gives u directly, and this was interpolated onto a regular grid with spacing 500 m in the horizontal and 100 m in the vertical. This spacing was chosen to correspond broadly to the spatial resolution of the radar data over the ranges used. The vertical velocity, w was calculated assuming that the billows were two dimensional by integrating the continuity equation (as described in CB) between the ground and 2 km, using a nine-point average around each grid box to smooth the u field. The quantities $< u >$ and $< w >$, taken as averages of u and w over the four billows between $x = 13.5$ and $x = 31.5$ km, and values of u^* and w^*, were calculated accordingly.

Figure 9 shows the $x - z$ cross-sections of (a) u^* and (b) w^* which were then combined to give (c) u^*w^*. The four billows all show the same qualitative structure in each of these fields. Although u^* and w^* vary with the same wavelength as the billows, the field of u^*w^* varies in the horizontal with a wavelength half that of the billow wavelength. For example, over billow IV between 27 and 31.5 km at a height of 1 km, u^*w^* shows a maximum, minimum, maximum then a minimum. There is a further set of maxima and minima at a height of 1.7 km, out of phase with those below. This is consistent with Fig. 13 of Busak and Brümmer (1987) who used a linear analytical model to simulate billows close to the ground. The u^*w^* field was averaged horizontally over each individual billow to give the four mean momentum flux profiles in Fig. 10. As might be expected from Fig. 9(c), profiles from billows I and II are similar to each other, as are profiles from III and IV. However, the latter pair have larger maxima and minima over the depth of the billows, and there is also a displacement in the vertical between the two pairs of profiles, such that the two pairs are approximately in anti-phase with each other. Good quality Doppler data were also available over two other billows (not shown); the momentum flux profiles from these are are qualitatively similar to the profiles from I and II.

Only two-dimensional eddies on horizontal scales between around 0.5 and 4 km can contribute to the momentum flux profiles calculated in this way, due to the resolution of the radar data and the way the vertical velocity is calculated. Thus it is only the effect of the main overturning of the billow on the mean velocity profile that is being measured, not the effect of its turbulent breakdown by eddies on smaller horizontal scales.

It is likely that a billow going through different stages of evolution would have different momentum flux profiles at each stage, which would account for some of the variation between the flux profiles in Fig. 10. This is supported by the numerical simulations by Fritts *et al.* (1996), which show that the momentum flux is strongest as the billows grow to maximum amplitude, but then fluctuates with time, even reversing in sign, before it decays to zero. In order to obtain an estimate of the net change in the mean wind profile from upstream to downstream of the billows, all six available momentum flux profiles were averaged. Although it was hoped thereby to sample the billows at six different stages in their evolution, it is not known how well they represent all stages in the evolution and so we have rather low confidence in the representivity of the average profile. The resulting profile is shown in Fig. 11(a), together with a smoothed profile. Smoothing was carried out so that small-scale

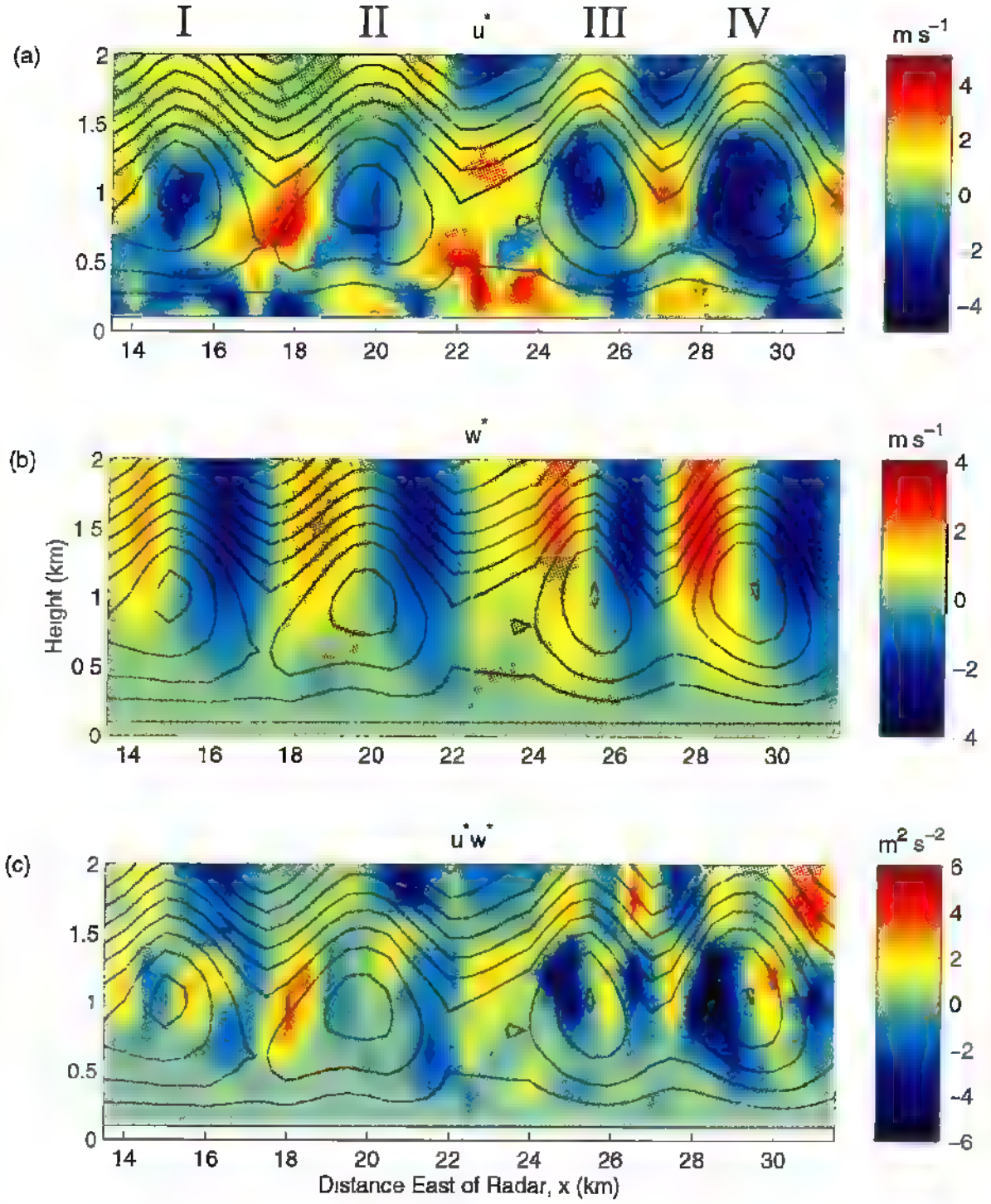

Figure 9: Radar-derived cross-sections through billows east of the radar at 2210 UTC, 6 September 1995, showing streamfunction (light solid contours) superimposed upon (a) u^* (m s^{-1}) (b) w^* (m s^{-1}) and (c) u^*w^* (m^2 s^{-2}). Roman numerals refer to individual billows.

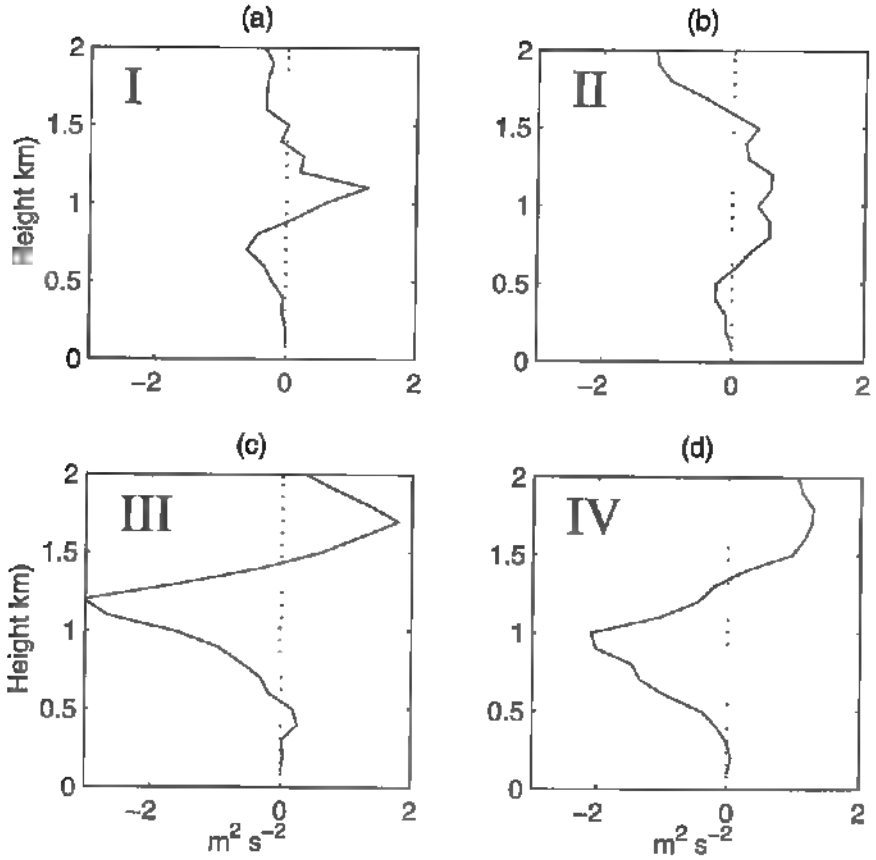

Figure 10: Momentum flux profiles averaged over the individual billows shown in Fig. 9.

fluctuations did not dominate in the derivation of the first and second vertical derivatives, as discussed in the following section.

(c) The effect of the momentum flux convergence on the mean wind shear profile

According to Eq. 3, the rate of change of the mean wind following the flow is given by the momentum flux convergence. Similarly, the rate of change of the mean wind shear following the flow is given by the vertical derivative of the momentum flux convergence. Averaged profiles of these two quantities, derived from Fig. 11(a), are plotted in Figs. 11(b) and 11(c), respectively. Equation 4 has been used to estimate the change in shear profile between locations 5 km south and 5 km north (solid and dashed curves, respectively, in Fig. 12(a)) of the original location of the profile. The shear responsible for the billows initially had a maximum at a height of 1.1 km, and was zero at 1.5 km. At 1.1 km, the vertical derivative of the momentum flux convergence was negative, indicating a tendency for the billows to reduce the peak shear at this height (see arrow in Fig. 12(a)). Between 1.3 and 1.8 km the vertical derivative of the momentum flux convergence was positive, indicating a tendency for the billows to increase the shear, thereby spreading the shear layer out over a greater depth in the vertical. The effect on the shear at lower levels (below 0.5 km) appears to have been considerably less.

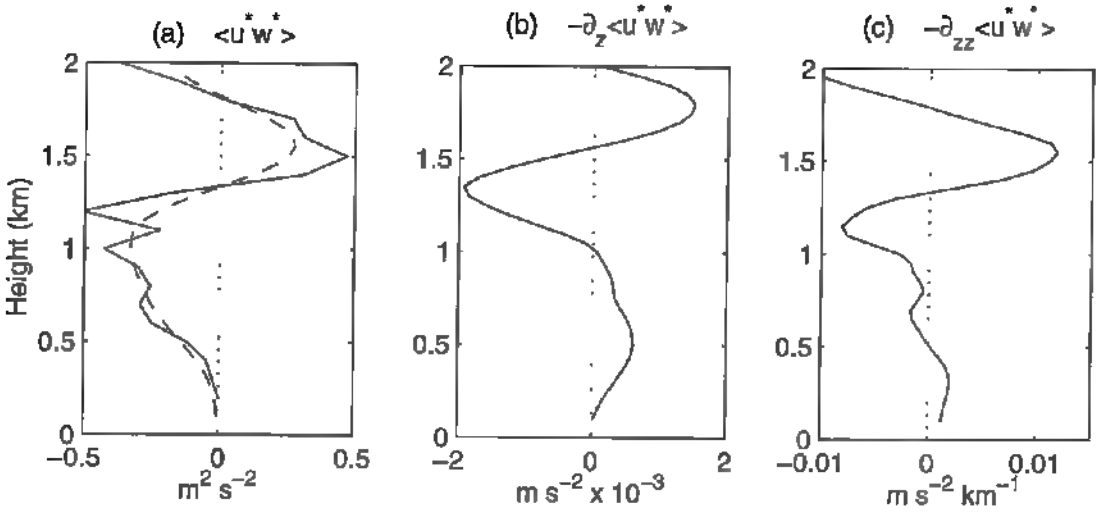

Figure 11: (a): Momentum flux profiles averaged over six billows (see text) east of radar between 2200 and 2220 UTC (solid line). Dashed line is a smoothed fit to the actual data. (b): Momentum flux convergence, derived from (a). (c): Vertical derivative of the momentum flux convergence, derived from (b).

(d) Comparison of calculated and observed profiles of wind shear upwind and downwind of the billows

The observed profiles of wind shear at locations towards the southern end and downwind of the billows separated by a distance of around 30 km are shown in Fig. 12(b). This separation is greater than that used above because of the interval between times when scans could be observed, as mentioned in Section 2(b). Reliable estimates of the wind shear profile could not be made as the train of billows move northwards during this interval. The trends in these profiles are in broad agreement with the trends in profiles inferred from momentum flux calculations, showing a decrease in peak shear, but an increase in shear above 1.4 km, and a smaller increase below 0.6 km. However, these results should be treated with caution, as there are a number of important sources of error:

- The calculation of w is susceptible to inaccuracy in two ways. Firstly the assumption of non-divergence in the south north direction may induce a systematic bias in the vertical velocity if this component of divergence is itself influenced by the billows. The nature of the radar data make it impossible to estimate the magnitude of this effect, although the variation of the south-north component of divergence in the west-east direction is unlikely to have been comparable to the west-east component of divergence itself. Secondly, the vertical velocity field was obtained by integrating upwards from as close to the ground as possible. However, at low levels the radar beam is contaminated by echos from the ground itself, so the level at which the integration was started (200 m) was relatively high, considering the low altitude of the billows. The effect of errors in w near the ground amplify with height, making this a potentially serious problem. The fields of w obtained are to a large extent validated only by qualitative comparison of the streamfunction with the original wind field. However, they do agree well with the prediction by Davis and Peltier (1976) that the maximum in the vertical velocity can occur higher than the critical level for the fastest growing instability when the shear layer is close to the ground.

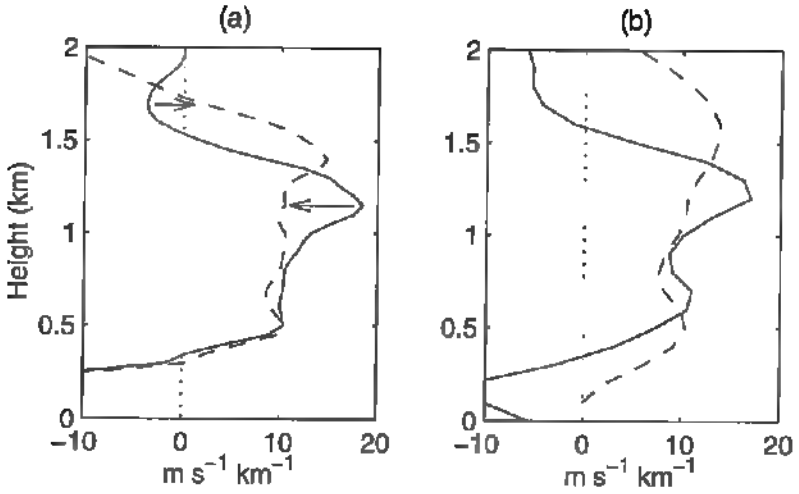

Figure 12: (a): Wind shear profiles at locations 5 km south and 5 km north (solid and dashed curves, respectively) of the initial shear profile, obtained by integrating the profile in Fig. 11(c). (b): Wind shear profiles measured within (solid lines) and downwind (dashed lines) of billows.

- The vertical velocity calculated represents only the main overturning of the billows, not the small-scale eddies involved in its turbulent breakdown. It is not obvious *a priori* which scale contributes most to the deepening of the shear layer, and how the contribution of each scale varies over the lifetime of the billows. However, three-dimensional numerical simulations by Fritts *et al.* (1996) indicate that it is mainly the overturning of the billow that affects the mean velocity profile, rather than smaller scale eddies associated with the breakdown of the billow, although these eddies influence the mean profiles indirectly via the evolution of the billow itself. This suggests that the method used here should, in principle, allow measurement of the momentum fluxes responsible for the change in mean shear profile over the lifecycle of billows.

- The sample of six billows is too small to show whether the variation seen in the individual momentum flux profiles is due to variation in the actual billow structure, or due to random errors. Even if the former were true, the sample size would still be too small for a reliable estimate of a representative average momentum flux profile over the lifetime of the billows.

In spite of these potentially large errors, the results are self-consistent. We are of the opinion that although the closeness of the agreement may be fortuitous, the results support the view that the overturning of the billows may indeed have been responsible for a large part of the observed change in wind shear profile over the length of the billows.

5 Overall discussion and significance of the results

This paper has described an observational study of large-amplitude billows which occurred over a distance between 50 and 90 km north of a strong surface warm front. There are few published observations of large-amplitude Kelvin-Helmholtz billows in the atmosphere, and even fewer measurements of momentum flux profiles through them. In one such study

Bryant and Browning (1975) used Doppler radar to investigate billows occurring at heights between 1 and 3 km within a warm frontal zone. They used very different methods from those described here to estimate the vertical flux of horizontal momentum. Whereas the billows in the present study had a wavelength of 4 to 5 km, those in the earlier study had a wavelength of 1 to 2 km. The magnitude of the resolved momentum flux had a maximum of around 0.1 $m^2\ s^{-2}$ in the shear layer, compared with 0.5 $m^2\ s^{-2}$ estimated here. This difference is what might be expected in view of the larger wavelength of the billows observed in the present study.

In another study of Kelvin Helmholtz billows, Blumen (1984) used wind and temperature measurements from an instrumented tower to calculate turbulent momentum fluxes due to billows in two occasions of night-time drainage winds. During periods when billows existed and the wind shear profile was observed to become smoothed with time, then the momentum fluxes acted in such a way as to cause this smoothing. The fluxes had a maximum of around 0.2 $m^2\ s^{-2}$ which is less than those calculated here. Again, this would be consistent with the smaller wavelengths (100-200 m) observed by Blumen.

The momentum fluxes estimated in the present study are of a similar magnitude to those observed in CAT at upper levels. For example, Kennedy and Shapiro (1979) found that the magnitude of the momentum flux within a number of upper level turbulence zones was between around 0 and 4 $m^2\ s^{-2}$. Trout and Panofsky (1969) used clear-air turbulence spectra and clear-air turbulence probabilities to show that the dissipation of energy by CAT between 25,000 and 40,000 ft is around 1 watt m^{-2}, which is not unimportant in the dynamics of the atmospheric circulation.

The most robust and important result in this paper is that the large amplitude billows were observed in a location just north of a surface warm front, which coincided with the onset of saturation due to ascent at the surface front. The onset of saturation suddenly lowered the Richardson number of a deep sheared layer in the frontal zone from around 1 to a value much less than $\frac{1}{4}$. The presence of saturation in the frontal zone was critical not only to the location but probably also to the amplitude of the billows that developed. In the absence of the sudden development of instability over a deep layer due to the onset of saturation, and in the absence of a rapid dynamically-induced increase in shear, it is likely that a critical Richardson number and associated billows would appear first over a shallower layer or layers.

The dependence of the dynamic stability of a stratified shear layer on its saturation is analogous to conditional instability (CI), which describes the dependence of the static stability of a parcel on its saturation. A temperature profile exhibits CI at a particular height if the air is statically stable at that height when the air is unsaturated, and statically unstable when the air is saturated, ie

$$\Gamma_{sat} < \Gamma < \Gamma_{dry}$$

where Γ_{sat}, Γ and Γ_{dry} represent the saturated, environmental and dry lapse rates $(-\partial T/\partial z)$, respectively. Likewise, a combined temperature and velocity profile exhibits what we may define as conditional shearing instability (CSHI) at a particular height if the air is dynamically stable at that height when the air is unsaturated, and dynamically unstable when the air is saturated, ie

$$Ri_{sat} < Ri_{crit} < Ri_{dry}$$

where Ri_{dry} and Ri_{sat} represent the gradient Richardson Number calculated assuming the air is dry and saturated using values of static stability calculated from Eqs. 1 and 2, respectively. Ri_{crit} represents the critical Richardson Number, which will in general be a little less than $\frac{1}{4}$.

Similarly there is an analogy between potential instability (PI) and what we define as potential shearing instability (PSHI). PI exists over a layer in the atmosphere when the layer would be statically unstable if it were lifted to saturation. This might occur if the lower part of the layer became saturated before the upper part. The condition for PI to exist is $\partial\theta_w/\partial z < 0$. PSHI exists over a layer if the layer would become dynamically unstable, but not statically unstable, when it is lifted to saturation (assuming the shear over the layer remains constant). The layer does not need to exhibit CSHI at its original height for this to occur (although it may do) as the lower part of the layer may become saturated before the upper part due to a vertical gradient in relative humidity. This could dynamically destabilise the layer, without making it statically unstable.

In the case described, flow into the region containing billows was along the contours of the front-parallel component of wind (Fig. 4), indicating that the shear over the layer which became responsible for the billows was conserved as the layer was lifted to saturation. This layer therefore exhibited PSHI upstream of the billows, as well as CSHI. The concept of PSHI allows us to see that a dynamically stable layer can exhibit a latent dynamical instability. Only through lifting to saturation can this instability be released. This could, for example, also occur in a layer forced to ascend over or downwind of orography, making billows visible on the edges of orographic clouds (e.g. Reiter *et al.* 1969).

The warm front described, although a strong one associated with an ex tropical cyclone, is not extraordinary, either in terms of the wind shear across it, or of the thermodynamic structure. It therefore seems likely that PSHI would exist and be released in many other warm fronts where ascent at the surface front induces saturation. Although billows are difficult to observe, there are a small number of published observations which appear to support this hypothesis. For example, Browning *et al.* (1970) made Doppler radar observations in two precipitating warm frontal zones. Fairly large amplitude billows (with wavelengths up to 5 km) were observed ahead of the surface warm front, and can be seen in a cross-section parallel to the surface front in Fig. 7 of their paper. The billows observed by Bryant and Browning (1975) using Doppler radar occurred in a precipitating warm frontal zone, just ahead of the surface front. The layer containing billows had been brought to saturation at the time when they were observed. They were orientated perpendicular to the surface front, and, again, were caused by the component of shear parallel to the front. Takahashi *et al.* (1993) observed large-amplitude billows within a precipitating shear layer orientated parallel to a stationary surface front. Wang *et al.* (1983) observed long wavelength (12-19 km) billows within a precipitating warm frontal zone. They noted that the Richardson number calculated over the layer containing billows was sub-critical only if the effect of moisture was included.

In addition to these previously published observations and the main case study presented in this paper, Figs. 1(d) and (e) of this paper show RHIs of Doppler velocity and vertical shear obtained in another warm frontal case on 11 February 1997. The billows apparent in these RHIs again occurred in a precipitating warm frontal zone just ahead of the surface warm front. The mesoscale model's representation of this front (not shown) revealed that

the air entering the region containing billows had been lifted to saturation by ascent at the warm front, although in this case the level of saturation was very close to the ground.

Studies of turbulent dissipation of kinetic energy in the free atmosphere have tended to concentrate on the dissipation by CAT, which is most likely to occur at upper level frontal zones and near the tropopause close to jets. The stronger winds at upper levels than at lower levels might at first appear to suggest that the energy dissipation in the free atmosphere would be dominated by the contribution from higher levels. However, strong shears also occur in low-level frontal zones and the onset of saturation near surface fronts allows PSHI to be released over large depths, so significant mixing may occur. The frequency of occurrence of billows in surface fronts, and a quantitative estimate of the mixing that they induce should be the subject of further research. This study has been restricted to warm fronts. Strong mixing also occurs within Kelvin-Helmholtz billows near the density-current head within sharp cold fronts, although here the sudden onset of saturation is not an issue.

Acknowledgements

We are grateful to Drs. Anthony Illingworth and Mark Blackman for their part in the data acquisition, and thank the Radio Communications Research Unit at Rutherford Appleton Laboratory for access to the Chilbolton radar. We are also grateful to Peter Panagi for supplying the Mesoscale Model data. Daniel Chapman is supported by a studentship from the Natural Environment Research Council.

References

Atlas, D., Metcalf, J. I., Richter, J. H., and Gossard, E. E. (1970). The birth of CAT and microscale turbulence. *J. Atmos. Sci.*, **27**, 903–913.

Blumen, W. (1984). An observational study of instablity and turbulence in nighttime drainage winds. *Boundary Layer Meteorol.*, **28**, 245–269.

Bosart, L. F. and Garcia, O. (1974). Gradient Richardson profiles and changes within an intense mid-tropospheric baroclinic zone. *Q. J. R. Meteorol. Soc.*, **100**, 593 607.

Browning, K. A. (1971). Structure of the atmosphere in the vicinity of large-amplitude Kelvin-Helmholtz billows. *Q. J. R. Meteorol. Soc.*, **97**, 283–299.

Browning, K. A. and Watkins, C. D. (1970). Observations of clear-air turbulence by high power radar. *Nature*, **227**, 260–263.

Browning, K. A., Harrold, T. W., and Starr, J. R. (1970). Richardson number limited shear zones in the free atmosphere. *Q. J. R. Meteorol. Soc.*, **96**, 40 49.

Browning, K. A., Bryant, G. W., Starr, J. R., and Axford, D. N. (1973a). Air motion within Kelvin-Helmholtz billows determined from simultaneous doppler radar and aircraft measurements. *Q. J. R. Meteorol. Soc.*, **99**, 619–638.

Browning, K. A., Hardman, M. E., Harrold, T. W., and Pardoe, C. W. (1973b). The structure of rainbands within a mid-latitude depression. *Q. J. R. Meteorol. Soc.*, **99**, 215–231.

Bryant, G. W. and Browning, K. A. (1975). Multi-level measurements of turbulence over the sea during the passage of a frontal zone. *Q. J. R. Meteorol. Soc.*, **101**, 35–54.

Busak, B. and Brümmer, B. (1987). A case study of Kelvin-Helmholtz waves within an offshore stable boundary layer: Observations and linear model. *Boundary Layer Meteorol.*, **44**, 105–135.

Chapman, D. and Browning, K. A. (1997). Radar observations of wind-shear splitting within evolving atmospheric Kelvin Helmholtz billows. *Q. J. R. Meteorol. Soc.*, **123**, 1433 1439.

Cullen, M. J. P. (1993). The unified forecast/climate model. *Met. Mag.*, **122**, 81–94.

Davis, P. A. and Peltier, W. R. (1976). Resonant parallel shear instability in the stably stratified planetary boundary layer. *J. Atmos. Sci.*, **33**, 1287–1300.

Drazin, P. and Reid, W. (1981). *Hydrodynamic Stability*. Cambridge University Press.

Durran, D. and Klemp, J. (1982). On the effects of moisture on the Brunt-Väisälä frequency. *J. Atmos. Sci.*, **39**, 2152–2158.

Fritts, D. C. and Garten, J. F. (1996). Wave breaking and transition to turbulence in stratified shear flows. *J. Atmos. Sci.*, **53**, 1057–1085.

Fritts, D. C., Palmer, T. L., Andreassen, O., and Lie, I. (1996). Evolution and breakdown of Kelvin-Helmholtz billows in stratified compressible flows. Part I: Comparison of two- and three-dimensional flows. *J. Atmos. Sci.*, **53**, 3173–3191.

Goddard, J. W. F., Eastment, J. D., and Thurai, M. (1994). The Chilbolton advanced meteorological radar: A tool for multidisciplinary research. *Electronics and Communications Engineering Journal*, **6**, 77–86.

Gossard (1990). Radar research on the Atmospheric Boundary Layer. Chapter 27a in *Radar in Meteorology*. Ed. D. Atlas. American Meteorological Society, pages 477–527.

Hardy, K. R., Reed, R. J., and Mather, G. K. (1973). Observation of Kelvin Helmholtz billows and their meso-scale environment by radar, instrumented aircraft and a dense radiosonde network. *Q. J. R. Meteorol. Soc.*, **99**, 279–293.

James, P. K. and Browning, K. A. (1981). An observational study of primary and secondary billows in the free atmosphere. *Q. J. R. Meteorol. Soc.*, **107**, 351–365.

Keller, J. L. (1989). Clear air turbulence as a response to meso- and synoptic-scale dynamic processes. *Mon. Wea. Rev.*, **18**, 2228–2242.

Kennedy, P. J. and Shapiro, M. A. (1979). Further encounters with clear air turbulence in research aircraft. *J. Atmos. Sci.*, **37**, 986–993.

Lalas, D. P. and Einaudi, F. (1974). On the correct use of the wet adiabatic lapse rate in stability criteria of a saturated atmosphere. *J. Appl. Meteorol.*, **13**, 318–324.

Ludlam, F. H. (1967). Characteristics of billows clouds and their relation to clear air turbulence. *Q. J. R. Meteorol. Soc.*, **93**, 419–435.

Ludlam, F. H. (1980). *Clouds and Storms.* Pensylvania State University Press.

Metcalf, J. I. and Atlas, D. (1973). Microscale ordered motions and atmospheric structure associated with thin echo layers in stably stratified zones. *Boundary Layer Meteorol.*, **4**, 7–35.

Miles, J. W. and Howard, L. N. (1964). Note on a heterogeneous shear flow. *J. Fluid Mech.*, **20**, 331–336.

Nielsen, J. W. (1992). In situ observations of Kelvin-Helmholtz waves along a frontal inversion. *J. Atmos. Sci.*, **49**, 369 386.

Readings, C. J. (1973). The formation and breakdown of Kelvin-Helmholtz billows (Working Group Report). *Boundary Layer Meteorol.*, **5**, 233–240.

Reiter, E. R., Lester, P. F., and Wooldridge, G. (1969). Spectral analysis of a breaking wave. *Clear Air Turbulence and its Detection,* Y.-H. Pao and A. Goldberg. Eds., Plenum Press, 21–33.

Roach, W. T. (1970). On the influence of synoptic development on the production of high level turbulence. *Q. J. R. Meteorol. Soc.*, **96**, 413–429.

Scinocca, G. P. (1995). The mixing of mass and momentum by Kelvin-Helmholtz billows. *J. Atmos. Sci.*, **52**, 2509–2530.

Sykes, R. I. and Lewellen, W. S. (1982). A numerical study of breaking Kelvin-Helmholtz billows using a Reynolds-stress turbulence closure model. *J. Atmos. Sci.*, **39**, 1506–1520.

Takahashi, N., Uyeda, H., and Kikuchi, K. (1993). A Doppler radar observation on wave-like echoes generated in a strong vertical shear. *J. Meteorol. Soc. Japan*, **71**, 357 365.

Thorpe, S. A. (1975). Turbulence in stably stratified fluids: A review of laboratory experiments. *Boundary Layer Meteorol.*, **5**, 95–119.

Thorpe, S. A. (1987). Transitional phenomena and the development of turbulence in strat ified fluids: A review. *J. Geophys. Res.*, **92**, 5231 5248.

Trout, D. and Panofsky, H. A. (1969). Energy dissipation near the tropopause. *Tellus*, **3**, 355–358.

Wang, P.-Y., Parsons, D. B., and Hobbs, P. V. (1983). The mesoscale and microscale structure and organization of clouds and precipitation in midlatitude cyclones. VI: Wavelike rainbands associated with a cold-frontal zone. *J. Atmos. Sci.*, **40**, 543–558.

CURRENT JCMM INTERNAL REPORTS

This series of JCMM Internal Reports, initiated in 1993, contains unpublished reports and also versions of articles submitted for publication. The complete set of Internal Reports is available from the National Meteorological Library on loan, if required.

1. **Research Strategy and Programme**
   K A Browning et al
   January 1993

2. **The GEWEX Cloud System Study (GCSS)**
   GEWEX Cloud System Science Team
   January 1993

3. **Evolution of a mesoscale upper tropospheric vorticity maximum and comma cloud from a cloud-free two dimensional potential vorticity anomaly**
   K A Browning
   January 1993

4. **The Global Energy and Water Cycle**
   K A Browning
   July 1993

5. **Structure of a midlatitude cyclone before occlusion**
   K A Browning and N Roberts
   July 1993

6. **Development in Systems and Tools for Weather Forecasting**
   K A Browning and G Szejwach
   July 1993

7. **Diagnostic study of a narrow cold frontal rainband and severe winds associated with a stratospheric intrusion**
   K A Browning and R Reynolds
   August 1993

8. **Survey of perceived priority issues in the parametrizations of cloud-related processes in GCMs**
   K A Browning
   September 1993

9. **The Effect of Rain on Longwave Radiation**
   I Dharssi
   September 1993

10. **Physical Cloud Microprocesses - A Description of the Parametrization used in the Large Eddy Model**
    H Swann
    July 1994

11. **An Appreciation of the Meteorological Research of Ernst Kleinschmidt**
    A J Thorpe
    May 1992

12. **Potential Vorticity of Flow Along the Alps**
    A J Thorpe, H Volkert and Dietrich Heimann
    August 1992

13. **The Representation of Fronts**
A J Thorpe
January 1993

14. **A Parametrization Scheme for Symmetric Instability: Test for an Idealised Flow**
C S Chan and A J Thorpe
February 1993

15. **The Fronts 92 Experiment: a Quicklook Atlas**
Edited by T D Hewson
November 1993

16. **Frontal wave stability during moist deformation frontogenesis**
Part 1. Linear wave dynamics
C H Bishop and A J Thorpe
May 1993

17. **Frontal wave stability during moist deformation frontogenesis**
Part 2. The suppression of non-linear wave development
C H Bishop and A J Thorpe
May 1993

18. **Gravity waves in sheared ducts**
C Bishop and A J Thorpe
November 1993

19. **Potential Vorticity and the Electrostatics Analogy: Quasi-Geostrophic Theory**
C Bishop and A J Thorpe
November 1993

20. **Recent Advances in the Measurement of Precipitation by Radar**
A J Illingworth
April 1993

21. **Micro-Physique et Givrage. Cloud Microphysics and Aircraft Icing**
A J Illingworth
May 1993

22. **Differential Phase Measurements of Precipitation**
M Blackman and A J Illingworth
May 1993

23. **Estimation of Effective Radius of Cloud Particles from the Radar Reflectivity**
N I Fox and A J Illingworth
May 1993

24. **A Simple Method of Dopplerising a Pulsed Magnetron Radar**
A Hau, A J Illingworth and J Eastment
November 1993

25. **Radiation and Polar Lows**
George C Craig
February 1994

26. **Collected preprints submitted to the International Symposium on the Life Cycles of Extratropical Cyclones; Bergen, Norway, 27 June - 1 July 1994**
April 1994

27. **Convective Frontogenesis**
Douglas J Parker and Alan J Thorpe
April 1994

28. **Improved Measurement of the Ice Water Content in Cirrus Using a Total Water Evaporator**
Philip R A Brown and Peter N Francis
April 1994

29. **Mesoscale Effects of a Dry Intrusion within a Vigorous Cyclone**
K A Browning and B W Golding
April 1994

30. **GEWEX Cloud System Study, Science Plan**
May 1994

31. **Parametrization of Momentum Transport by Convectively Generated Gravity Waves**
R Kershaw
February 1995

32. **Mesoscale Modelling Newsletter No 5**
May 1994

33. **Observations of the mesoscale sub-structure in the cold air of a developing frontal cyclone**
K A Browning, S A Clough, C S A Davitt, N M Roberts and T D Hewson
May 1994

34. **Longwave Radiative Forcing of a Simulated Tropical Squall Line**
Imtiaz Dharssi
July 1994

35. **On the nature of the convective circulation at a kata-cold front**
K A Browning
September 1994

36. **Collective preprints of papers submitted to the COST-75 International Seminar on Advanced Weather Radar Systems, Brussels, 20-23 September 1994**
November 1994

37. **Use of satellite imagery to diagnose events leading to frontal thunderstorms: Parts 1 and 11 of a case study**
K A Browning and N M Roberts
November 1994

38. **The role of spaceborne millimetre-wave radar in the global monitoring of ice cloud**
P R A Brown, A J Illingworth, A J Heymsfield, G M McFarquahar, K A Browning and M Gosset
December 1994

39. **Potential Vorticity Inversion**
Michael Ziemianski
October 1994

40. **Theory of mature tropical cyclones; a comparison between Kleinschmidt (1951) and Emanuel (1986)**
Suzanne L Gray
December 1994

41. **Dispersion and removal of pollutants during the passage of an atmospheric frontal System**
N R Gimson
December 1994

42. **The role of snow sublimation in frontogenesis**
D J Parker and A J Thorpe
December 1994

43. **Potential vorticity and the electrostatics Analogy: Ertel- Rossby formulation**
A J Thorpe and C H Bishop
December 1994

44. **Mesoscale aspect of extratropical cyclones: an observational perspective**
K A Browning
January 1995

45. **A Polar Low Outbreak: Evolution and Mesoscale Structures**
T D Hewson, G C Craig and C Claud
February 1995

46. **Generation of near-surface gusts of deep convection**
K Nakamura and R Kershaw
April 1995

47. **Attribution Concepts applied to the Omega Equation**
S A Clough, C S A Davitt and A J Thorpe
June 1995

48. **Parametrization of mixed-phase cloud and precipitation**
Susan P Ballard and M Gerard Hutchinson
June 1995

49. **Short-range forecasting of stratocumulus: Initialization Prediction**
Susan Ballard, Simon D Jackson and B Macpherson
June 1995

50. **Contributions of the JCMM/Dept of Meteorology Radar Group to the 27th AMS Radar Meteorology Conference, Vail October 1995**
June 1995

51. **Cold Pools in Shear**
Douglas J Parker
September 1995

52. **High-resolution analysis of frontal fracture**
K A Browning, S P Ballard and C S A Davitt
September 1995

53. **The Albedo of Broken Cloud Fields: Calculations using a modified two stream radiation code**
Imtiaz Dharssi and Roy Kershaw
October 1995

54. **Parametrization of momentum transport by convection. I: Theory and cloud modelling results**
R Kershaw and D Gregory
November 1995

55. **Variation of frontal structure along a cold front**
K A Browning and N M Roberts
November 1995

56. **Secondary Frontal Waves**
Douglas Parker
December 1995

57. **Objective Fronts**
T D Hewson
March 1996

58. **Mesoscale analysis of the activation of a cold front during cyclogenesis**
K A Browning, N M Roberts and A J Illingworth
June 1996

59. **Investigation of Different Representations of Rain in a 1-d Evaporation Model**
H Swann
May 1996

60. **Parametrization of diabatic processes in the inversion of the omega-equation**
M Athanassiadou and A J Thorpe
June 1996

61. **The Role of the Environmental Flow in the Development of Secondary Frontal Cyclones**
I A Renfrew, A J Thorpe and A Joly
June 1996

62. **Consequences of the geostrophic momentum approximation on barotropic instability**
S Malardel, A J Thorpe and A Joly
June 1996

63. **Contributions to the AMS/RMS Conference on Mesoscale Processes**
Reading, 9-13 September 1996

64. **Vorticity and Potential Vorticity in Stratified Flows Interacting with an Isolated Obstacle**
Jorge A Gutiérrez and A J Thorpe
September 1996

65. **Triple Point Development: Two Case Studies**
Douglas Parker
September 1996

66. **Radar observations of wind-shear splitting within evolving atmospheric Kelvin-Helmholtz billows**
D Chapman and K A Browning
April 1997

67. **Cold Frontal Structure derived from radar wind profilers**
K A Browning, D Jerrett, J Nash, T Oakley, N M Roberts
May 1997

68. **The dry intrusion and its effect on the frontal, cloud and precipitation structure of extratropical cyclones**
K A Browning - Text of invited special lecture at the Spring Conference of the Meteorological Society of Japan, University of Tsukuba, 22 May 1997

69. **Met. Office Unified Model data, diagnostic graphics programs, and other observational data available from the JCMM through the aegis of the Universities Weather Research Network (UWERN).** Plus supplement.
Peter Panagi and Ed Dicks
June 1997

70. **Contributions of the JCMM/Dept of Meteorology Radar Group to 28th AMS Radar Meteorology Conference.** Austin, Texas
September 1997

71. **Sensitivity of short-range weather forecasts to local potential vorticity modifications**
Meral Demirtas and Alan Thorpe
July 1997

72. **Objective identification of frontal wave cyclones**
T D Hewson
August 1997

73. **Attribution and its application to mesoscale structure associated with tropopause folds**
A J Thorpe
September 1997

74. **The Role of the Environmental Flow in the Development of Secondary Frontal Cyclones**
Ian A Renfrew, Alan J Thorpe and Craig H Bishop
September 1997

75. **Potential Vorticity: A short history of its definitions and uses**
Alan J Thorpe and Hans Volkert
September 1997

76. **Superposing Semi-Geostrophic Potential Vorticity Anomalies**
H R Birkett and A J Thorpe
September 1997

77. **Short period forecasting of catchment-scale precipitation.**
Part 1: the role of Numerical Weather Prediction
M A Pedder, M Haile and A J Thorpe
September 1997

78. **Verification of the Tracking Technique Used in an Experimental Cloud Motion Wind Inferring System**
Z Wang, K A Browning and G A Kelly
October 1997

79. **A Preliminary Study of Fourier Series Analysis for Cloud Tracking with GOES High Temporal Resolution Images**
Z Wang
October 1997

80. **Analysis of an ex-tropical cyclone after reintensifying as a warm-core extratropical cyclone**
K A Browning, G Vaughan and P Panagi
November 1997

81. **A JCMM overview of FASTEX IOPs**
S A Clough, H W Lean, N M Roberts, H Birkett, J-P Chaboureau, R Dixon, M Griffiths, T D Hewson and A Montani
January 1998

82. **Programs for PV Inversion and modification**
Meral Demirtas
December 1997

83. **Release of potential shearing instability in warm frontal zones**
D Chapman and K A Browning
February 1998

Met Office Joint Centre for Mesoscale Meteorology Department of Meteorology
University of Reading PO Box 243 Reading RG6 6BB United Kingdom
Tel: +44 (0)118 931 8425 Fax: +44 (0)118 931 8791
www.metoffice.com